RSC Advances

ROYAL SOCIETY OF CHEMISTRY

www.rsc.org/advances

ARTICLE TYPE www.rsc.org/xxxxxx | XXXXXXXX

A facile solution-based approach to photocatalytic active branched one-dimensional TiO_2 array

Jin-Ming Wu*[a] and Jia-Xing Yin[a]

Received (in XXX, XXX) Xth XXXXXXXXX 200X, Accepted Xth XXXXXXXXX 200X
First published on the web Xth XXXXXXXXX 200X
DOI: 10.1039/b000000x

Branched one-dimensional TiO_2 array with rutile nanorods growing radially around anatase nanowires was fabricated via a facile solution-based strategy. The remarkably enhanced photocatalytic activity was attributed to the abundant surface hydroxyl groups, nitrogen doping, surface sulfating, increased light harvesting, high specific surface area, and anatase/rutile phase junctions.

Materials with three-dimensional (3D) nanostructures exhibit excellent performances in the various fields of green energy, energy storage, and photocatalysis.[1-7] It is reported that, as an anode material for lithium ion battery (LIB), hierarchical SnO_2 nanostructures constructed from 2D nanosheets exhibited superior reversible capacities and improved cyclic capacity retention when compared with commercial SnO_2 nanoparticles.[5] A "nanoforest" of high density, long-branched hierarchical ZnO nanowires significantly increased the conversion efficiency of a dye-sensitized solar cell (DSSC).[6] One of the feasible techniques to construct 3D nanostructures is to precipitate a wide range of compounds on previously obtained 1D nanomaterials.[7-13] The 1D nanostructure can be fabricated by various methods based on vapor liquid solid (VLS), template based and electrochemically induced growth.[14,15]

Titania (TiO_2) is among the important semiconductors finding wide applications in photocatalysis,[16-19] sensors,[20] water splitting,[21-23] LIBs,[24] and DSSCs[9,25-27]. Various techniques, including but not limited to, hydrothermal[8,9,23,27] or solvothermal synthesis,[12] acid vapor oxidation[28-30], and pulsed laser deposition[31] have been developed to fabricate 3D hierarchical TiO_2 arrays. For example, Yang et al. developed a one-pot approach to grow rutile TiO_2 nanotrees via the reaction of a titanium surface with an acidic vapor generated from a HCl solution in an autoclave at 140 °C.[28,29] After a final calcination at 500 °C, anatase TiO_2 nanotrees can also be fabricated by treating at 100 °C the hydrogen titanate ($H_2Ti_2O_5 \cdot H_2O$) nanorods in an autoclave filled with 0.02 M H_2SO_4.[30] Chu et al. reported the one-pot hydrothermal fabrications of anatase TiO_2 nanotrees on various metal wires of Ti, W, Ni, etc., which exhibited satisfying performances when utilized as photoanodes in DSSCs.[9]

Hydrogen titanates with 1D nanostructures, which serve as precursors to synthesize 1D nanostructured TiO_2, are generally adopted by alkali-hydrothermal treatments of metallic Ti plates or TiO_2 particles, followed by a proton-exchange procedure. Recently, we developed a facile solution procedure to fabricate vertically aligned 1D titanate nanowires on arbitrary substrates.[32] Utilizing such 1D titanate nanowires as precursors, we herein report a simple yet effective approach to achieve branched 1D TiO_2 arrays. The reaction between metallic Ti foils and a H_2O_2 solution precipitated directly titanate nanowire array at 80 °C and under the atmospheric pressure, requiring neither autoclaves nor complicated proton-exchange procedures. Experimental details are provided in the online Electronic Supplementary Information, ESI†. As demonstrated in Scheme 1, the as-synthesized titanate nanowire array (see Fig. S1a for the field emission scanning electron microscopy, FESEM, image) was subjected to an intermediate calcination in air at moderate temperatures of 240-260 °C, which in situ introduced poorly crystallized anatase that acted as the seeds for the growth of the branches during a subsequent H_2SO_4 (0.01 M) treatment at 80 °C for up to 72 h. The titanate nanowire procursor serves both as a trunk and as a reactant for the radially growth of the rutile branches.

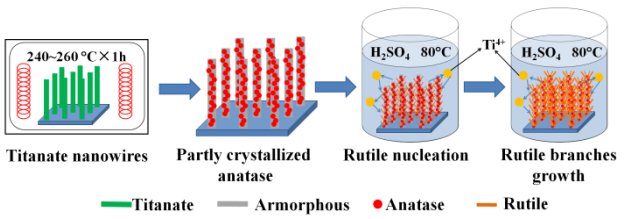

Scheme 1 A schematic image demonstrating the formation of the branched 1D TiO_2.

Figures 1a and 1b show FESEM images of the branched nanowires covering homogeneously the Ti substrate. The cross-sectional FESEM image indicates that the thickness of the branched nanowire layer was ca. 1 μm. There existed a 1 μm- thick layer between the branched top layer and the substrate, which consisted of compact nanoparticles (Fig. 1c).

A transmission electron microscopy (TEM) image showing typically the radially growth of nanorods along the surface of a nanowire is demonstrated in Fig. 1d. The average diameter of the nanorod branch is ca. 12 nm and the length is ca. 44 nm. The high-resolution TEM (HRTEM) image of the branches was illustrated in Fig. 1f. It can be seen that each branch was a single-crystalline nanorod. The inter-plane spaces of ca. 0.33 nm can be attributed to the (110) crystal plane of rutile TiO_2. The nanowire trunk consisted of many grains (Fig. 1g). The fringe with inter-plane spaces of ca. 0.35 nm can be assigned to the (101) crystal plane of anatase TiO_2. The TEM characterizations thus suggest that, the branched 1D TiO_2 consisted of well-crystallized single-crystalline rutile

TiO_2 branches, which grew outside along the polycrystalline anatase TiO_2 nanowires. The corresponding selected area electron diffraction (SAED) pattern provides an additional support for such a phase composition (Fig. 1e).

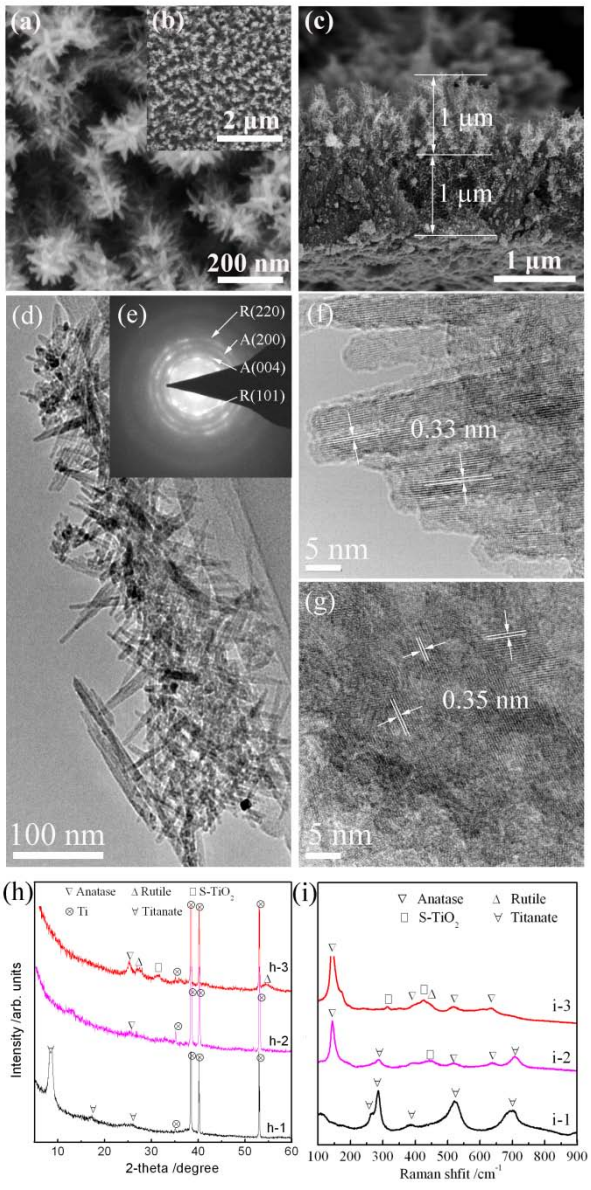

Fig. 1 FESEM (a-c), TEM (d), HRTEM (f, g) images, and SAED pattern (e) of the branched 1D TiO_2, which was achieved by calcinating the titanate nanowires at 260 °C and followed by a final H_2SO_4 treatment at 80 °C for 72 h. XRD patterns (h) and Raman spectra (i) for the as-synthesized titanate nanowires (h-1, i-1), those after an intermediate calcination at 260 °C (h-2, i-2), and followed by a final H_2SO_4 treatment at 80 °C for 72 h (h-3, i-3).

The X-ray diffraction (XRD) pattern of the as-synthesized nanowires (Fig. 1, h-1) demonstrates diffraction peaks at about 8.6°, 17.2°, and 25.9° in 2θ, which could be indexed to the (200), (400), and (600) crystal faces of a hydrogen titanate $H_2Ti_5O_{11}{\cdot}3H_2O$, according to the JCPDS card NO. 44-0130. The Raman analysis confirmed the ascription of the as-synthesized nanowire array (Fig. 1, i-1). After calcination in air at 260 °C for 1 h, the diffraction peaks of $H_2Ti_5O_{11}{\cdot}3H_2O$ disappeared and a tiny XRD peak located at around 25.3° in 2θ, which corresponds to anatase TiO_2, can be discerned (Fig. 1, h-2). The corresponding Raman spectrum suggested more clearly the coexistence of hydrogen titanate and anatase TiO_2, together with a weak peak corresponding to srilankite TiO_2 (Fig. 1, i-2). It thus indicated that calcination at 260 °C resulted in the decomposition of $H_2Ti_5O_{11}{\cdot}3H_2O$ to poorly crystallized anatase TiO_2. The final H_2SO_4 treatment led to a mixed phase of anatase, rutile, and trace srilankite for the branched 1D TiO_2 (Fig. 1, h-3 and i-3), which is in accordance with the TEM characterizations.

The morphology evolution of the branched 1D TiO_2 is illustrated in Fig. 2. The intermediate calcination at 260 °C induced no significant change in the morphology (Fig. 2a). After 12 h, tiny nanorods can be seen surrounding the nanowire surface (Fig. 2b), which grew further upon the prolonged duration to 24 h (Fig. 2c) and 72 h (Fig. 1a).

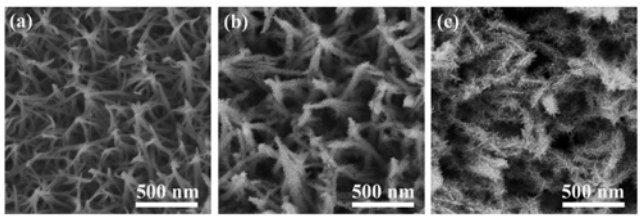

Fig. 2 FESEM surface morphologies for thin films of titanate nanowires after an intermediate calcination at 260 °C (a), and those followed by final H_2SO_4 treatments at 80 °C for 12 h (b) and 24 h (c).

The present branched 1D TiO_2 can be achieved only when the intermediate calcination was carried out at 240-260 °C (Fig. S2). When the calcination temperature was lower than 240 °C, the subsequent H_2SO_4 treatment changed titanate nanowires in part to rutile TiO_2 nanoflowers (Fig. S3a and Fig. S4a). When the calcination temperature was beyond 300 °C, titanate nanowires decomposed predominantly to anatase TiO_2, together with trace srilankite TiO_2 (Fig. S5). In comparison with the unstable titanate nanowires, such anatase nanowires are resistance to the subsequent H_2SO_4 treatment and no remarkable change in both morphology (Fig. S1b, S3b) and phase composition (Fig. S4b) can be discerned.

Based on the results above-mentioned, the formation procedure of the present branched 1D TiO_2 can be argued as follows. In the acidic environment, the titanate nanowires were attacked readily by H_2SO_4 to release hydrated Ti(IV) ions into the solution, which, once reached a critical concentration, would precipitate back to the metallic Ti substrate to form TiO_2. The formation of rutile is favored in an acidic environment;[33] therefore, tiny rutile nanorods formed, which assembled to form 3D rutile nanoflowers via an oriented attachment mechanism for the titanate nanowires calcinated at a temperature lower than 240 °C (Fig. S3a). The sulfate ions play key role in the formation of the branched 3D nanoflowers.[34] In case that HCl was utilized instead of H_2SO_4, titanate nanowires changed to aligned rutile nanorods.[35] The appropriate intermediate calcination at 240-260 °C decomposed the titanate to poorly crystallized anatase (Fig. 1, h-2 and i-2). It is reasonable to assume that the calcination made the nanowires more resistant to the attack of H_2SO_4,

because the 300 °C-heated anatase nanowires remained unchanged upon the subsequent H_2SO_4 treatment (Figs. S3b and S4b). A reduced Ti(IV) concentration in the H_2SO_4 solution can thus be anticipated when the nanowires were subjected to the intermediate calcination at 240-260 °C. As a result, a heterogeneous nucleation of the tiny rutile nanorods along the poorly crystallized nanowires was favored. In the other word, the tiny anatase crystallites in the nanowire trunk served as seeds for the nucleation and growth of the rutile TiO_2 branches. Arrays of hierarchical nanostructures with anatase trunks surrounded by rutile branches, which possessed many surface anatase/rutile phase junctions, were thus constructed simply yet effectively by the present low temperature solution approach.

Figure 3 shows the XPS analysis results of the branched 1D TiO_2. The binding energy of Ti 2p is observed at 464.2 eV and 458.4 eV, which is assigned to the spectrum of Ti $2p_{1/2}$ and Ti $2p_{3/2}$. The separation between these two peaks is 5.8 eV, which is in agreement with the XPS data in the literature.[36] A shoulder peak located at 1.5 eV towards the lower binding energy of Ti $2p_{3/2}$ can also be discerned, which can be attributed to Ti^{3+} in pure Ti_2O_3. [34,37] As shown in Fig 3b, the O 1s spectrum can be devolved into two contributions, the main band of O 1s at 529.8 eV is assigned to the lattice oxygen (Ti-O-Ti), and the contribution at around 531.2 eV belongs to the O_{Ti}^{3+}.

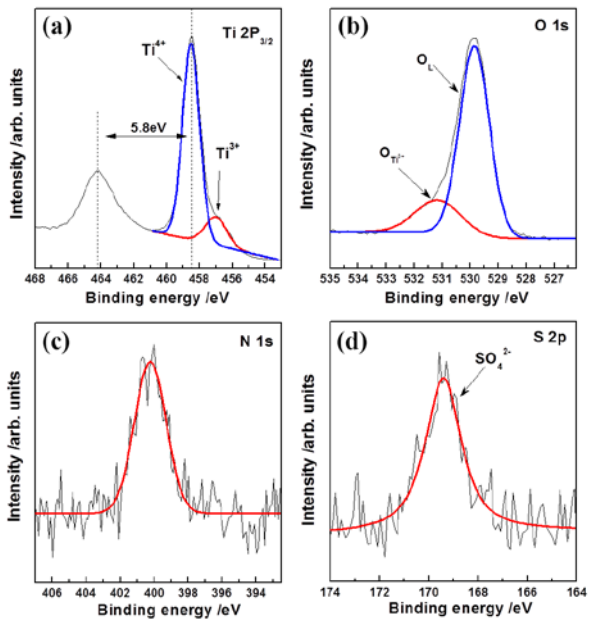

Fig. 3 High resolution Ti 2p, O 1s, N 1s, and S 2p XPS spectra for the branched 1D TiO_2, which was achieved by calcinating the titanate nanowires at 260 °C and followed by a final H_2SO_4 treatment at 80 °C for 72 h.

Trace elements of nitrogen (Fig. 3c) and sulfur (Fig. 3d) can also be detected by XPS for the branched 1D TiO_2. The binding energy of N 1s is around 399.2 eV, which can be attributed to N-O, N-N, or N-C bonds, as a result of the melamine decomposition during the fabrication of the titanate nanowires.[32] After the H_2SO_4 treatment, sulfate ions also incorporated into the titania film, which gave the peak at 169.4 eV.[34,38]

Figure 4a shows the UV-Vis diffuse reflectance spectra of the rutile nanoflowers (HS), branched 1D TiO_2 (HS260), and anatase nanowires (HS300). The branched 1D TiO_2 exhibited significantly a lower reflectance over the visible light region. The band gap of TiO_2 can be estimated by extrapolating the tangent line in the plot of $\alpha^{1/2}$ against $h\nu$, where α is the absorption coefficient and $h\nu$ is the photon energy.[39] Fig. 4b indicates that, the anatase nanowire array possessed an indirect bandgap of ca. 3.15 eV, which is slightly lower than that of bulk anatase TiO_2 (E_g = 3.2 eV). The branched 1D TiO_2 possessed a much lower bandgap of 3.05 eV, which can be attributed to the increasing amount of rutile in the film. It is argued that the presence of Ti^{3+} generates sublevels with energy lower than the conduction band of minimum (CBM) of stoichiometric titania.[37,40,41] The XPS measurement illustrates the presence of significant surface Ti^{3+} ions in the branched 1D TiO_2 (Fig. 3a), which might be a result of the nitrogen doping[42,43]. This explains the result that, although the branched 1D TiO_2 consisted mainly of anatase, its bandgap is much nearer to that of rutile TiO_2 (E_g = 3.0 eV). The bandgap of the 3D rutile nanoflower (2.97 eV) was near to that of bulk rutile.

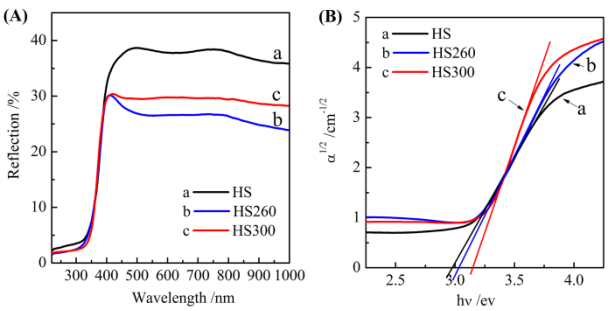

Fig. 4 (A) UV-Vis spectra for thin films of the titanate nanowires after the final H_2SO_4 treatments at 80 °C for 72 h, without (a, HS) and with an intermediate thermal treatment at 260 °C (b, HS260) and 300 °C (c, HS300). (B) Re-plotting of (A) in the $\alpha^{1/2}$~hν coordinates to estimate the corresponding band gap, assuming an indirect transition between bands for TiO_2.

The photoctalytic activity was evaluated by photodegradations of aqueous sulfosalicylic acid (SSA) with an initial concentration of 10 mg/L, into which 20 ppm H_2O_2 was added to accelerate the photocatalytic reaction. Fig. 5a indicates the photodegradation curve of SSA in the presence of the 3D rutile nanoflowers (HS), branched 1D TiO_2 (HS260), and anatase nanowires (HS300 and HT450). The blank test revealed no significant degradation of SSA under the UV light illumination and in the presence of 20 ppm H_2O_2 only. Fig 5b shows that, all the degradation kinetics followed roughly a pseudo-first-order reaction,

$$-\ln(c/c_0) = kt \qquad \text{Eq. (1)}$$

where c_0 and c represent the initial SSA concentration and that after light illumination for a duration t, respectively. The apparent reaction rate constant (k), which was defined by the slope of the straight lines through zero as shown in Fig. 5b,

was 0.613, 1.899, 0.778, and 0.986 × 10^{-2} min^{-1} for the films HS, HS260, HS300, and HT450. Obviously, the branched 1D TiO_2 exhibited the highest photocatalytic activity in assisting photodegradation of SSA in water, which induced nearly a thorough degradation of SSA after 2 h (Fig. S6).

The rutile nanoflowers (HS) exhibited the poorest efficiency to assist photodegradation of SSA in water, which might be attributed to the well-established fact that, for photocatalytic reactions utilizing dissolved oxygen as the electron acceptor, rutile exhibits an activity lower than that of anatase.[44] The anatase nanowire array achieved by calcination at 450 °C (HT450) possessed a slightly higher activity than that achieved by calcination at 300 °C and followed by the H_2SO_4 treatment (HS300). This can be explained by the higher crystallinity that inhibits the recombination of photogenerated charges. Interestingly, the branched 1D TiO_2 (HS260) possessed a photocatalytic activity almost doubled that of the anatase nanowires (HS300 and HT450), which evidenced the advantages of the branched 1D nanostructure.

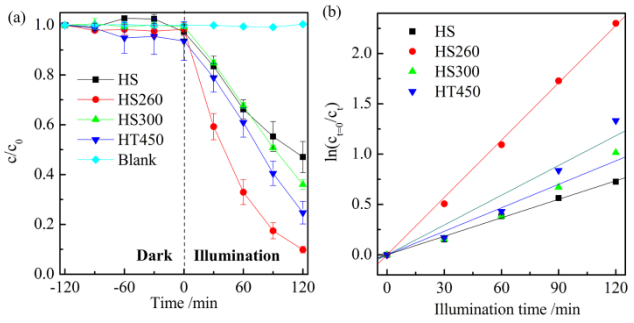

Fig. 5 Photodegradation curves of SSA in water in the presence of the various TiO_2 thin films: (a) the degradation curves and (b) the fitting results assuming a pseudo-first order reaction. Three parallel tests were performed to give the error bar in (a). The nanowire film achieved by calcination of the as-synthesized titanate nanowire array in air at 450 °C for 1 h (HT450) was included for comparison purpose. Refer to Fig. 4 for the ascriptions of HS, HS260 and HS300.

Titania with 1D nanofeatures exhibited unique performances when compared with nanoparticles; yet it still suffers from several neagative aspects, such as a relatively low specific surface area, a smooth surface, a single crystal phase, and a broad bandgap.[13] The present branched 1D TiO_2 overcame effectively the above-mentioned drawbacks. The XPS analysis suggested significant surface oxygen deficiencies and in turn abundant surface hydroxyl groups (Fig. 3a, b), which have been argued to favor the photodegradation of the organics in water.[45] Nitrogen doping, which is a widely adopted tactic to improve the photocatalytic activity of titania under visible light illumination, can also be discerned (Fig. 3c). The incorporation of sulfate ions in TiO_2 (Fig. 3d) may also benefit the photodegradation procedure, because it improves surface acidities and promotes the formation of hydroxyl groups on the catalyst surface as well.[46] The branched architecture favors the diffuse reflectance and hence an improved absorption of the incident light (Fig. 4). The rutile nanorods growing radially along the nanowires increased the specific surface area and hence produced more active sites, which play key roles in the photocatalytic reactions. More importantly, the branched 1D TiO_2 consisted of anatase trunks that are surrounded by rutile branches, which is thus full of anatase/rutile surface phase junctions. An optimized mixture of anatase and rutile has been reported to facilitate the charge separation and hence the photocatalytic activity because of a phase juction effect.[47,48]

The present technique to fabricate branched 1D TiO_2 array requires neither high temperature nor high pressure, which is extremely suitable for a scale-up production. The titanate nanowire precursor can be deposited on arbitaray substrates;[32] the branched 1D TiO_2 array may thus find wide applications in green energy and environment remediations.

Conclusions

A facile solution based technique was developed for mass fabrications of branched 1D TiO_2 array under the atmospheric pressure. A hydrogen titanate nanowire array was firstly adopted by a non-hydrothermal Ti-H_2O_2 reaction at a low temperature of 80 °C on metallic Ti substrates. The hydrogen titanate nanowires decomposed to poorly crystallized anatase TiO_2 after an intermediate calcination at 240-260 °C for 1 h in air, which, after simply immersing in a H_2SO_4 solution at 80 °C for 12-72 h, achieved the branched 1D TiO_2 array. The branched 1D TiO_2 consisted of single-crystalline rutile TiO_2 nanorods (branches), which grew radially along the trunk of polycrystalline anatase nanowires. When utilized to assist photodegradation of sulfosalicylic acid in water, the branched 1D TiO_2 exhibited an efficiency doubled that of the anatase nanowire array. The enhanced photocatalytic activity can be attributed to the many merits of abundant surface hydroxyl groups, nitrogen doping, surface sulfating, increased light harvesting, high specific surface area, and surface anatase/rutile phase junctions.

Acknowledgements

This work is funded by Zhejiang Provincial Natural Science Foundation of China under Grant No. LY13E020001.

Notes and references

[a] *State Key Laboratory of Silicon Materials and Department of Materials Science and Engineering, Zhejiang University, Hangzhou 310027, P. R. China. *Corresponding author, Fax: +86-571-87953115; E-mail: msewjm@zju.edu.cn*

† Electronic Supplementary Information (ESI) available: Detailed experimental procedures, additional XRD patterns, Raman spectra, and FESEM images. UV-Vis adsorption spectra of SSA in the presence of the branched 1D TiO_2 and under the UV light illumination for various durations. See DOI: 10.1039/b000000x/

1. A. Javey, S. W. Nam, R. S.Friedman, H. Yan, C. M. Lieber, *Nano Lett.*, 2007, **7**, 773.
2. K. S. Park, J. G. Kang, Y. J. Choi, S. Lee, D. W. Kim, J. G. Park, *Energy Environ. Sci.*, 2011, **4**, 1796.
3. F. H. Zhao, J. G. Zheng, X. F. Yang, X. Y. Li, J. Wang, F. L. Zhao, K. S. Wong, C. L. Liang, M. M. Wu, *Nanoscale*, 2010, **2**, 1674.
4. W. Wen, J. M. Wu, *RSC Adv.*, 2014, **4**, 58090.
5. H. B. Wu, J. S. Chen, X. W. Lou, H. H. Hng, *J. Phys. Chem. C*, 2011, **115**, 24605.

6. S. H. Ko, D. Lee, H. W. Kang, K. H. Nam, J. Y. Yeo, S. J. Hong, C. P. Grigoropoulos, H. J. Sung, *Nano Lett.*, 2011, **11**, 666.
7. S. Park, S. Lee, S. W. Seo, S. D. Seo, C. W. Lee, D. Kim, D. W. Kim, K. S. Hong, *CrystEngComm*, 2013, **15**, 2939.
8. Y. J. Chen, C. L. Zhu, X. L. Shi, M. S. Cao, H. B. Jin, *Nanotechnology*, 2008, **19**, 205603.
9. L. Chu, L. Y. Li, J. Su, F. F. Tu, N. H. Liu, Y. H. Gao, *Sci. Rep.*, 2014, **4**, Art. No. 4420.
10. J. Shi, Y. Hara, C. Sun, M. A. Anderson, X. D. Wang, *Nano Lett.*, 2011, **11**, 3413.
11. U. K. Gautam, X. S. Fang, Y. Bando, J. H. Zhan, D. Golberg, *ACS Nano*., 2008, **2**, 1015.
12. Q. J. Zhang, C. H. Sun, J. Yan, X. J. Hu, S. Y. Zhou, P. Chen, *Solid State Sci*., 2010, **12**, 1274.
13. J. Tian, Z. H. Zhao, A. Kumar, R. I. Boughton, H. Liu, *Chem. Soc. Rev*., 2014, doi: 10.1039/c4cs00180j.
14. S. V. N. T. Kuchibhatla, A. S. Karakoti, D. Bera, S. Seal, *Prog. Mater. Sci*., 2007, **52**, 699.
15. X. D. Wang, Z. D. Li, J. Shi, Y. H. Yu, *Chem. Rev.*, 2014, doi: dx.doi.org/10.1021/cr400633s.
16. J. B. Joo, I. Lee, M. Dahl, G. D. Moon, F. Zaera, Y. Yin, *Adv. Funct. Mater*., 2013, **23**, 4246.
17. D. Wang, T. C. Hu, L. T. Hu, B. Yu, Y. Q. Xia, F. Zhou, W. M. Liu, *Adv. Funct. Mater.*, 2009, **19**, 1930.
18. L. L. Lai, L. L. Huang, J. M. Wu, *RSC Adv.*, 2014, **4**, 49280.
19. J. G. Wang, X. R. Li, J. Zhu, H. X. Li, *Nanoscale*, 2013, **5**, 1876.
20. K. Fischer, S. G. Mayr, *Adv. Mater.*, 2011, **23**, 3838.
21. A. Fujishima, K. Honda, *Nature*, 1972, **238**, 37.
22. K. Lee, R. Hahn, M. Altomare, E. Selli, P. Schmuki, *Adv. Mater.*, 2013, **25**, 6133.
23. I. S. Cho, Z. B. Chen, A. J. Forman, D. R. Kim, P. M. Rao, T. F. Jaramillo, X. L. Zheng, *Nano Lett.*, 2011, **11**, 4978.
24. G. Kim, C. Jo, W. Kim, J. Chun, S. Yoon, J. Lee, W. Choi, *Energy Environ. Sci.*, 2013, **6**, 2932.
25. W. G. Wang, H. Y. Zhang, R. Wang, M. Feng, Y. M. Chen, *Nanoscale*, 2014, **6**, 2390.
26. R. H. Tao, J. M. Wu, H. X. Xue, X. M. Song, X. Pan, X. Q. Fang, X. D. Fang, S. Y. Dai, *J. Power Sources*, 2010, **195**, 2989.
27. M. R. Subramaniam, S. Devanathan, D. Kumaresan, *RSC Adv.*, 2014, **4**, 36791.
28. X. F. Yang, J. L. Zhuang, X. Y. Li, D. H. Chen, G. F. Ouyang, Z. Q. Mao, Y. X. Han, Z. H. He, C. L. Liang, M. M. Wu, J. C. Yu, *ACS Nano*, 2009, **3**, 1212.
29. X. F. Yang, C. J. Jin, C. L. Liang, D. H. Chen, M. M. Wu, J. C. Yu, *Chem. Commun.*, 2011, **47**, 1184.
30. F. Shao, J. Sun, L. Gao, S. W. Yang, J. Q. Luo, *J. Mater. Chem.*, 2012, **22**, 6824.
31. F. Sauvage, F. D. Fonzo, A. L. Bassi, C. S. Casari, S. Russo, G. Divitini, C. Ducati, C. E. Bottani, P. Comte, M. Grätzel, *Nano Lett.*, 2010, **10**, 2562.
32. B. Li, J. M. Wu, T. T. Guo, M. Z. Tang, W. Wen, *Nanoscale*, 2014, **6**, 3046.
33. M. P. Finnegan, H. Z. Zhang, J. F. Banfield, *J. Phys. Chem. C*, 2007, **111**, 1962.
34. J. Sun, W. Wen, J. M. Wu, *J. Am. Ceram. Soc.*, 2013, **96**, 2109.
35. J. Sun, J. M. Wu, *Sci. Adv. Mater.*, 2013, **5**, 549.
36. L. Qin, X. X. Pan, L. Wang, X. P. Sun, G. L. Zhang, X. W. Guo, *Appl. Catal. B: Environ.*, 2014, **150–151**, 544.
37. M. S. Hamdy, R. Amrollahi, G. S. Mul, *ACS Catal.*, 2012, **2**, 2641.
38. F. Berger, E. Beche, R. Berjoan, D. Klein, A. Chambaudet, *Appl. Surf. Sci*., 1996, **93**, 9.
39. E. Sanchez, T. Lopez, *Mater. Lett.*, 1995, **25**, 271.
40. X. B. Chen, L. Liu, P. Y. Yu, S. S. Mao, *Science*, 2011, **331**, 746.
41. S. Hoang, S. P. Berglund, N. T. Hahn, A. J. Bard, C. B. Mullins, *J. Am. Chem. Soc.*, 2012, **134**, 3659.
42. G. D. Yang, T. Wang, B. L. Yang, Z. F. Yan, S. J. Ding, T. C. Xiao, *Appl. Surf. Sci*., 2013, **287**, 135.
43. G. D. Yang, Z. Jiang, H. H. Shi, T. C. Xiao, Z. F. Yan, *J. Mater. Chem.*, 2010, **20**, 5301.
44. T. Ohno, K. Sarukawa, M. Matsumura, *J. Phys. Chem. B*, 2001, **105**, 2417.
45. Y. Shiraishi, N. Saito, T. Hiral, *J. Am. Chem. Soc.*, 2005, **127**, 12820.
46. X. C. Wang, J. C. Yu, P. Liu, X. X. Wang, W. Y. Su, X. Z. Fu, *J. Photochem. Photobiol. A.*, 2006, **179**, 339.
47. J. Zhang, Q. Xu, Z. C. Feng, M. J. Li, C. Li, *Angew. Chem. Int. Ed.*, 2008, **47**, 1790.
48. K. L. Schulte, P. A. DeSario, K. A. Gray, *Appl. Catal. B: Environ.*, 2010, **97**, 354.